INTERNATIONAL JOURNAL FOR NUMERICAL METHODS IN ENGINEERING
Int. J. Numer. Meth. Engng 2000; **49**:653–668

One-dimensional analysis of thin-walled closed beams having general cross-sections

Jin Hong Kim[†,‡] and Yoon Young Kim[*,§,¶]

School of Mechanical and Aerospace Engineering and Institute of Advanced Machinery and Design, Seoul National University, Kwanak-Gu, Shinlim-Dong, San 56-1, Seoul 151-742, Korea

SUMMARY

This paper presents a new one-dimensional theory for static and dynamic analysis of thin-walled closed beams with general cross-sections. Existing one-dimensional approaches are useful only for beams with special cross-sections. Coupled deformations of torsion, warping and distortion are considered in the present work and a new approach to determine sectional warping and distortion shapes is proposed. One-dimensional C^0 beam elements based on the present theory are employed for numerical analysis. The effectiveness of the present theory is demonstrated in the analysis of thin-walled beams having pillar sections of automobiles and excavators. Copyright © 2000 John Wiley & Sons, Ltd.

KEY WORDS: thin-walled closed beam; general cross-section; one-dimensional analysis; finite element

1. INTRODUCTION

Thin-walled closed beams have been widely used as efficient load-carrying structural members. However, a practically simple yet accurate structural theory for such beams with general cross-sections has not been developed. Detailed plate/shell finite element analysis gives satisfactory results, but is not practical from the viewpoint of initial beam design. For instance, the initial design and analysis of thin-walled closed automobile pillars is usually based on one-dimensional beam models.

Simplified one-dimensional analysis is preferred over two-dimensional plate/shell analysis not only because the one-dimensional analysis is efficient but also because it gives greater freedom in thin-walled beam section design. This has motivated the present authors and we are presenting a new one-dimensional theory for static and dynamic analysis of thin-walled closed beams having *general* cross-sections. Analyses for rectangular [1] and quadrilateral [2] cross-sections have been reported earlier by the present authors.

*Correspondence to: Yoon Young Kim, Department of Mechanical Design and Production Engineering, Seoul National University, Shinlim Don San 56-1, Kwanak-Gu, Seoul 151-742, Korea
†Research Associate
‡E-mail: nockim@idealab.snu.ac.kr
§Associate Professor
¶E-mail: yykim@snu.ac.kr

Received 14 May 1999
Revised 9 November 1999

Most complete analysis on thin-walled closed beams was carried out by Vlasov [3] who pioneered thin-walled beam analysis. The analysis for extension, bending and flexure is rather straightforward, but the analysis for the coupled deformations of torsion, warping and distortion poses a major challenge. Subsequently, recent work on thin-walled beams is focused on the latter, which is also the subject of the present investigation. Maisel and Roll [4], and Maisel [5] also give excellent reviews on the same subject. Kim and Kim [2] list a number of important references on the analysis of coupled deformations [6–15], but there is no existing theory for arbitrarily shaped cross-sections.

The key analysis in developing one-dimensional theories for the coupled-deformation analysis is to find correctly and efficiently cross-sectional deformation shapes associated with distortion among other deformation patterns. Thus simple and accurate determination of the shapes is critical in establishing a satisfactory one-dimensional approach. From this viewpoint, it is worth mentioning Maisel's work [5], which may be applied for general sections. Maisel [5] attempted to describe the cross-sectional deformation shape associated with distortion, usually referred to as a distortion function. The limitation of his approach is that the polygonal cross-section of a thin-walled beam was simply viewed as a hinged system. Therefore, his distortion function did not satisfy rotation or moment continuities at the corners. As a result, his function is far from describing realistic sectional deformation, and Vlasov [3] points out the serious drawback of hinge systems in rectangular cross-sections. Although there are some investigations [6, 16] on simpler cross-sections such as trapezoidal sections, no satisfactory theory for general sections has been formulated yet.

In the present work, we first present a new beam-frame approach to determine the distortion function. The present distortion function is determined by solving an eigenvalue problem of a beam-frame of a given cross-section. The deformation of each segment of a polygonal cross-section (corresponding to each wall of the beam) is approximated by the deformation shape proposed earlier for a quadrilateral box beam [2]. Correct distortion functions are then obtained from the eigenmodes of the beam-frame system that are orthogonal to three rigid-body motions. The distortional warping functions can be then determined by considering the shear flows developed by the distortional deformations.

Another important issue arises in the case of cross-sections with more than four corners since there exist several distortion patterns. We argue that the minimum number of deformation functions is two and the technique to determine such functions is also developed. Unlike distortional and distortional warping deformations, torsional and torsional warping deformations in a cross-section can be obtained easily by following the same procedure used for quadrilateral cross-sections [2].

Utilizing the sectional deformation functions newly derived in this work, a one-dimensional theory for general cross-sections is established. Actual numerical calculations are performed by developing C^0 beam finite elements. Practically important cross-sections, such as automobile pillar sections, are considered for numerical examples in order to show the effectiveness of the present theory.

2. BASIC FIELD EQUATION AND ASSUMPTION

We describe the shell displacement of a point on the contour in terms of the normal $u_n(s,z)$, tangential $u_s(s,z)$ and axial $u_z(s,z)$ components as indicated in Figure 1. The same assumptions presented previously by Kim and Kim [1, 2] are adopted here. The beam deformation measures at a given axial co-ordinate z are denoted by the amounts of rotation $\theta(z)$, torsional warping $U^{\theta}(z)$,

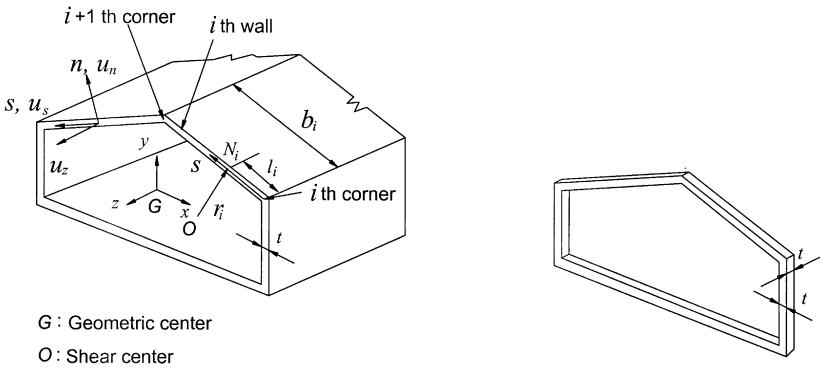

(a) (b)

Figure 1. (a) A general thin-walled closed beam; and (b) the corresponding beam-frame model.

distortion $\chi(z)$ and distortional warping $U^{\chi}(z)$. For general cross-sections, however, there may be more than one set of distortion and distortional warping deformation shapes as we will see later. In terms of these sectional deformation shapes, one can write the shell displacement as the product of a function of s and a function of z:

$$u_s(s,z) = \psi_s^{\theta}(s)\theta(z) + \psi_s^{U^{\theta}}(s)U^{\theta}(z) + \psi_s^{U^{\chi}}(s)U^{\chi}(z) + \psi_s^{\chi}(s)\chi(z) \tag{1a}$$

$$u_n(s,z) = \psi_n^{\theta}(s)\theta(z) + \psi_n^{U^{\theta}}(s)U^{\theta}(z) + \psi_n^{U^{\chi}}(s)U^{\chi}(z) + \psi_n^{\chi}(s)\chi(z) \tag{1b}$$

$$u_z(s,z) = \psi_z^{\theta}(s)\theta(z) + \psi_z^{U^{\theta}}(s)U^{\theta}(z) + \psi_z^{U^{\chi}}(s)U^{\chi}(z) + \psi_z^{\chi}(s)\chi(z) \tag{1c}$$

In Equations (1), $\psi(s)$ represent sectional deformations in the n–s plane for unit values of $\theta, U^{\theta}, U^{\chi}$ and χ. The functions superscribed by θ and U^{θ} for the ith edge are given in Kim and Kim [2]:

$$\begin{aligned} &\psi_s^{\theta}(s) = r_i, \quad \psi_n^{\theta}(s) = -l_i + s, \quad \psi_z^{\theta}(s) = 0 \\ &\psi_s^{U^{\theta}}(s) = 0, \quad \psi_n^{U^{\theta}}(s) = 0, \quad \psi_z^{U^{\theta}}(s) = -\int_0^s (r_i - r_n)\,\mathrm{d}s + \psi_{z0}^{U^{\theta}} \\ &r_n = \frac{2A_1}{\oint \mathrm{d}s} \end{aligned} \tag{2}$$

In Equation (2), the distance of the normal ON_i from the shear centre O to the point N_i of the ith edge is denoted by r_i: see Figure 1(a). The area enclosed by and the total length of the contour are denoted by A_1 and $\oint \mathrm{d}s$, respectively. The length of each wall is denoted by b_i. The distance from the ith corner to the point N_i is denoted by l_i. The integration constant $\psi_{z0}^{U^{\theta}}$ is determined from the condition that average axial displacement must vanish.

It is worth examining the nature of distortional and distortional warping deformations for subsequent analysis. Note that distortional deformations are not accompanied by axial displacement:

$$\psi_s^{\chi}(s) \neq 0, \quad \psi_n^{\chi}(s) \neq 0, \quad \psi_z^{\chi}(s) = 0 \tag{3}$$

On the other hand, only the axial deformation is significant when distortional warping ($U^{\chi}(z)$) takes place:

$$\psi_s^{U^{\chi}}(s)=0, \quad \psi_n^{U^{\chi}}(s)=0, \quad \psi_z^{U^{\chi}}(s)\neq 0 \tag{4}$$

The approach to find the correct functional form of $\psi_s^{\chi}(s)$, $\psi_n^{\chi}(s)$ and $\psi_z^{U^{\chi}}(s)$ will be presented in the next section. Once the shell deformation of a cross-section is found, the corresponding three-dimensional displacements $\tilde{u}_n(n,s,z)$, $\tilde{u}_s(n,s,z)$, $\tilde{u}_z(n,s,z)$ can be obtained. On the assumption that the wall thickness is much smaller than the beam length, one can show [1, 2]

$$\tilde{u}_n(n,s,z) \approx u_n(s,z)=\psi_n^{\theta}(s)\theta(z)+\psi_n^{\chi}(s)\chi(z) \tag{5a}$$

$$\tilde{u}_s(n,s,z) \approx u_s(s,z)+n\frac{\partial u_n(s,z)}{\partial s} \approx \psi_s^{\theta}(s)\theta(z)+\psi_s^{\chi}(z)\chi(s)+n\frac{\mathrm{d}\psi_n^{\chi}(s)}{\mathrm{d}s}\chi(z) \tag{5b}$$

$$\tilde{u}_z(n,s,z) \approx u_z(s,z)=\psi_z^{U^{\theta}}(s)U^{\theta}(z)+\psi_z^{U^{\chi}}(s)U^{\chi}(z) \tag{5c}$$

The normal co-ordinate n in Equation (5b) is measured from the middle line of each wall. Non-negligible three-dimensional strain components obtained form the displacement in Equations (5) can be found as

$$\varepsilon_{zz} = \frac{\partial \tilde{u}_z}{\partial z} \approx \psi_z^{U^{\theta}}(s)\frac{\mathrm{d}U^{\theta}(z)}{\mathrm{d}z}+\psi_z^{U^{\chi}}(s)\frac{\mathrm{d}U^{\chi}(z)}{\mathrm{d}z} \tag{6a}$$

$$\varepsilon_{zs} = \frac{1}{2}\left(\frac{\partial \tilde{u}_z}{\partial s}+\frac{\partial \tilde{u}_s}{\partial z}\right) \approx \frac{1}{2}\left[\frac{\mathrm{d}\psi_z^{U^{\theta}}(s)}{\mathrm{d}s}U^{\theta}(z)+\frac{\mathrm{d}\psi_z^{U^{\chi}}(s)}{\mathrm{d}s}U^{\chi}(z)+\psi_s^{\theta}(s)\frac{\mathrm{d}\theta(z)}{\mathrm{d}z}+\psi_s^{\chi}(s)\frac{\mathrm{d}\chi(z)}{\mathrm{d}z}\right] \tag{6b}$$

$$\varepsilon_{ss} = \frac{\partial \tilde{u}_s}{\partial s} \approx n\frac{\mathrm{d}^2\psi_n^{\chi}}{\mathrm{d}s^2}\chi(z) \tag{6c}$$

3. A SEMI-ANALYTIC BEAM-FRAME APPROACH

This section gives a new approach to determine the distortion functions ($\psi_s^{\chi}(s), \psi_n^{\chi}(s)$) and the distortional warping function ($\psi_z^{U^{\chi}}(s)$) for general sections. Figure 1(a) shows a general thin-walled closed beam which consists of N_{w} walls. Each wall of the beam is assumed inextensional in the tangential direction. The shapes of the sectional deformations are assumed not to vary through the axial direction of the beam. Therefore, the sectional deformation shapes may be determined from a beam-frame model developed for a given beam cross-section: Figure 1(b) shows a typical beam-frame model. The beam frame is assumed to have the unit depth in the plane perpendicular to the cross-sectional plane.

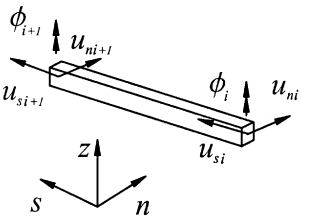

Figure 2. In-plane degrees of freedom of a member of a beam-frame model.

3.1. Distortion function

The present approach to determine distortion functions can be described by the following procedure.

Step 1: Assume the functional form of $\psi_s^\chi(s)$ and $\psi_n^\chi(s)$ as simple as possible. The functions $\psi_{si}^\chi(s)$ and $\psi_{ni}^\chi(s)$ $(i=1,\ldots,N_w)$ are defined in each wall. These functions must be selected so as to satisfy corner continuities.

Step 2: Develop the stiffness matrix of the beam-frame model, $\mathbf{K}_{BF}$ and solve the eigenproblem of the system in order to determine the corner values of the in-plane displacements and rotations corresponding to the lowest distortion modes.

Step 3: Use these corner values to determine explicitly the analytic form of $\psi_{si}^\chi(s)$ and $\psi_{ni}^\chi(s)$. These functions $\psi_{si}^\chi(s)$ and $\psi_{ni}^\chi(s)$ will be used in developing the present one-dimensional theory.

For *Step* 1, the approach developed for general quadrilateral sections by Kim and Kim [2] is extended for the present general section problems. Namely we assume the displacement field in the following form:

$$\psi_{si}^\chi(s) \approx \frac{u_{si+1}+u_{si}}{2} \tag{7a}$$

$$\psi_{ni}^\chi(s) \approx \left(-\frac{-2\phi_i-2\psi_{\theta i}^\chi}{b_i^2}-\frac{\phi_i-\phi_{i+1}}{b_i^2}\right)s^3 + \left(\frac{-3\phi_i-3\psi_{\theta i}^\chi}{b_i}+\frac{\phi_i-\phi_{i+1}}{b_i}\right)s^2+\phi_i s+\psi_{\theta i}^\chi\frac{b_i}{2}+\frac{u_{ni+1}+u_{ni}}{2} \tag{7b}$$

In Equations (7), u_{si} and u_{ni} denote the tangential and normal displacements at the ith corner. The rotations of the ith wall at the ith and $(i+1)$th corners are denoted by ϕ_i and ϕ_{i+1} (see Figure 2). The rotation of the ith wall as a rigid body, denoted by $\psi_{\theta i}^\chi$, can be written as

$$\psi_{\theta i}^\chi = \frac{-u_{ni+1}+u_{ni}}{b_i} \tag{8}$$

The relative ratios of the corner values of u_{ni}, u_{si}, ϕ_i $(i=1,\ldots,N_w)$, which actually determine section deformation shapes, were obtained analytically by Kim and Kim [2] for a quadrilateral cross-section. At the corners, all the displacement and rotation continuities were satisfied, but only the moment continuity was used as the first approximation. However, it is not only difficult but also

impractical to find distortion functions analytically in the case of general cross-sections because of complexity involved. This motivates the direct numerical determination of the corner values using a beam-frame finite element model for a given cross-section.

Before discussing a numerical procedure based on the beam-frame finite element model, we address the important properties that any distortion deformation shape must satisfy

$$\oint r\psi_s^{\chi}(s)\,\mathrm{d}A = \sum_{i=1}^{N_w} r_i b_i \psi_{si}^{\chi} \approx \sum_{i=1}^{N_w} r_i b_i \frac{u_{si+1}+u_{si}}{2} = 0 \tag{9a}$$

$$\oint \psi_s^{\chi}(s)\cdot\frac{\mathrm{d}x}{\mathrm{d}s}\,\mathrm{d}A = \sum_{i=1}^{N_w} b_i \psi_{si}^{\chi}\cos\,\alpha_i \approx \sum_{i=1}^{N_w} b_i \frac{u_{si+1}+u_{si}}{2}\cos\,\alpha_i = 0 \tag{9b}$$

$$\oint \psi_s^{\chi}(s)\cdot\frac{\mathrm{d}y}{\mathrm{d}s}\,\mathrm{d}A = \sum_{i=1}^{N_w} b_i \psi_{si}^{\chi}\sin\,\alpha_i \approx \sum_{i=1}^{N_w} b_i \frac{u_{si+1}+u_{si}}{2}\sin\,\alpha_i = 0 \tag{9c}$$

In Equations (9), α_i is the angle between the horizontal axis x and the tangent of the ith wall. The conditions stated by Equations (9) imply that the distortional stress produces no virtual work for any rigid-body virtual displacement. (See [2].) Equation (9a) is the condition for a rigid-body rotation whereas Equations (9b) and (9c) are, for two rigid-body translations.

Now we discuss a numerical procedure to determine the corner values of u_{si}, u_{ni}, ϕ_i $(i=1,\ldots,N_w)$ using a beam-frame model. This procedure corresponds to *Step* 2. A given cross-section is modelled by a beam-frame in which N_w plane beam elements are used to represent N_w walls. The tangential and normal displacements are approximated by linear and cubic polynomials, respectively, in the present beam elements. Note that the tangential displacements are approximated by piecewise linear functions in the beam-frame finite element model although only piecewise constant approximation is employed for the tangential displacement shape $\psi_{si}^{\chi}(s)$ in Equation (7a). This modification allows simpler numerical implementation because not only the moment but also force continuities at the corners can be satisfied and thus the subsequent numerical analysis does not suffer from the singularity problem of the resulting stiffness matrix. Once the corner values of u_{si}, u_{ni}, ϕ_i are determined from the beam-frame finite element model, these values are provided to determine ψ_{si}^{χ} and ψ_{ni}^{χ} in Equations (7).

Using the linear and cubic polynomial approximations for the distortion displacement field, the stiffness matrix $\mathbf{K}_{BF}$ of the beam-frame model can be constructed. The corresponding nodal displacement vector $\mathbf{u}$ is defined as

$$\mathbf{u} = \{u_{s1}, u_{n1}, \phi_1, \ldots, u_{sN_w}, u_{nN_w}, \phi_{N_w}\}^{\mathrm{T}} \tag{10}$$

The easiest way to find the distortional deformation shapes that satisfy Equations (9) is to set the following eigenvalue problem:

$$\mathbf{K}_{BF}\mathbf{u} = \lambda\mathbf{u} \tag{11}$$

where λ is the eigenvalue of the stiffness matrix $\mathbf{K}_{BF}$. The three rigid-body motions correspond to $\lambda = 0$, and the other eigenvectors, representing distortional deformation shapes, are automatically orthogonal to the rigid-body motions. The ith eigenvalue λ_i represents the strain energy of the

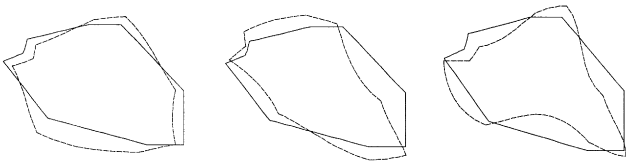

Figure 3. The three lowest eigenmodes of a pillar section of the beam shown in Figure 7(a).

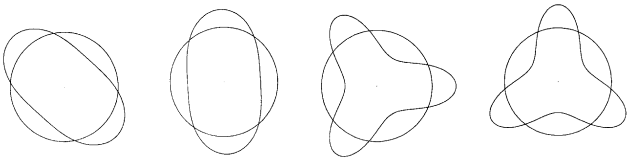

Figure 4. The four lowest eigenmodes of a circular ring.

corresponding eigenvector $\mathbf{u}_i$, which may be evident by examining the strain energy of the ith eigenvector

$$U_i = \tfrac{1}{2}\mathbf{u}_i^{\mathrm{T}}\mathbf{K}_{\mathrm{BF}}\mathbf{u}_i = \tfrac{1}{2}\lambda_i\mathbf{u}_i^{\mathrm{T}}\mathbf{u}_i = \tfrac{1}{2}\lambda_i \quad (\text{with } \mathbf{u}_i^{\mathrm{T}}\mathbf{u}_j = \delta_{ij}) \tag{12}$$

Therefore, the eigenvectors corresponding to lower eigenvalues have lower-energy deformation shapes. One may wonder what the crucial advantage of solving an eigenvalue problem stated in Equation (12) would be in seeking the sectional distortion shapes. To address this, we recall that unlike a quadrilateral section [2] that has only one distortional section deformation shape, general sections have more than one section deformation shape. For a cross-section shown in Figure 7(a), for instance, one can show that seven distortion shapes are obtained. Three of them are plotted in Figure 3, and these results are obtained from the solution of Equation (11). Since the use of all of the distortion shapes does not merit a one-dimensional analysis over a two-dimensional plate/shell analysis, a method to select the first few important shapes is required. We argue that the eigenvalue gives a best criterion to select important shapes; the shapes corresponding to lower eigenvalues can be selected.

Now we must determine how many deformation functions should be used. What is the minimum number of deformation functions? To answer this question, we propose to use only two distortional shapes for $N_{\mathrm{w}} \geqslant 5$. To support this proposition, we observe that a circular cross-section (i.e. a ring) may be viewed as a cross-section having an infinite number of walls ($N_{\mathrm{w}} \to \infty$). Figure 4 shows several in-plane deformation shapes of a ring, but the two lowest modes have the same eigenfrequency. Therefore, we can conclude that the use of only one distortion shape in a general section may not be sufficient to represent possible distortion patterns. Subsequently, we select the two lowest-energy modes for the present one-dimensional beam analysis. The problem of using only the lowest energy distortion shape will be addressed later in numerical examples.

Once one (for $N_{\mathrm{w}} = 4$) or two (for $N_{\mathrm{w}} \geqslant 5$) distortion functions are determined from the finite element solution of Equation (11), the corner values of u_{si}, u_{ni}, ϕ_i of each function are used to determine the analytic distortion functions (*Step* 3). The analytic distortion functions in

Equation (7) are extremely useful in deriving distortional warping functions. Furthermore, the analytic distortion functions facilitate the analytic derivation of one-dimensional system potential energy from three-dimensional potential energy (see Section 4).

3.2. *Distortional warping function*

Distortional warping is accompanied by in-plane distortional deformation. The stress state for non-uniform distortional deformation cannot be in equilibrium unless axial stress is produced by distortional warping deformation. As in the case of warping deformation associated with torsion, distortional warping deformation can produce a non-vanishing twisting moment, which may be characterized by a shear flow q. Based on this physical consideration, one may use the following expression to determine $u_z^{U^\chi}$:

$$q = Gt\left(\frac{\partial u_z^{U^\chi}}{\partial s} + \frac{\partial u_s^\chi}{\partial z}\right) \tag{13}$$

where $u_s^\chi = \psi_s^\chi \chi(z)$ as given by Equation (1a), and $\psi_s^\chi(s)$ is determined in the previous section. The unknown shear flow q may be determined by the singlevalueness requirement of the displacement $u_z^{U^\chi}$:

$$0 = \oint \mathrm{d}u_z^{U^\chi} = \frac{q}{G}\oint \frac{\mathrm{d}s}{t} - \frac{\mathrm{d}\chi}{\mathrm{d}z}\oint \psi_s^\chi \,\mathrm{d}s \tag{14}$$

The shear flow q is assumed to be independent of s in Equation (14) and $\oint$ represents the contour integral along the curve representing the middle line of the cross-section. Rearranging Equation (14), the shear flow q can be found as

$$q = G\frac{\oint \psi_s^\chi \,\mathrm{d}s}{\oint \dfrac{\mathrm{d}s}{t}}\frac{\mathrm{d}\chi}{\mathrm{d}z} \tag{15}$$

Substituting q in Equation (15) into Equation (13) yields

$$\frac{\partial u_z^{U^\chi}}{\partial s} \equiv \left[\bar{\psi}_s^\chi - \psi_s^\chi(s)\right]\frac{\mathrm{d}\chi}{\mathrm{d}z} \tag{16}$$

where $\bar{\psi}_s^\chi$ is defined as

$$\bar{\psi}_s^\chi \equiv \frac{\oint \psi_s^\chi \,\mathrm{d}s}{t\oint \dfrac{\mathrm{d}s}{t}} \tag{17}$$

If $u_z^{U^\chi}$ is assumed as (see Equation (1c))

$$u_z^{U^\chi}(s,z) = \psi_z^{U^\chi}(s)U^\chi(z) \tag{18}$$

and Equation (18) is substituted into Equation (16), one can see that

$$U^\chi(z) = \frac{\mathrm{d}\chi(z)}{\mathrm{d}z}$$

and

$$\psi_z^{U^\chi}(s) = \int_{s_0}^{s} \left[\bar{\psi}_s^{\chi} - \psi_s^{\chi}(s)\right] \mathrm{d}s + \psi_{z0}^{U^\chi}$$

$$\equiv \hat{\psi}_z^{U^\chi}(s) + \psi_{z0}^{U^\chi} \tag{19}$$

in which $\hat{\psi}_z^{U^\chi}$ is defined as

$$\hat{\psi}_z^{U^\chi}(s) = \int_{s_0}^{s} [\bar{\psi}_s^{\chi} - \psi_s^{\chi}(s)] \, \mathrm{d}s \tag{20}$$

To determine the constant $\psi_{z0}^{U^\chi}$, one may use the condition that the distortional warping stress ($= E_1 \partial u_z^{U^\chi}/\partial z$) produces no virtual work for any rigid-body axial virtual displacement:

$$\oint \psi_z^{U^\chi}(s) t \, \mathrm{d}s = 0 \tag{21}$$

Substituting Equation (19) into Equation (21) determines $\psi_{z0}^{U^\chi}$ as

$$\psi_{z0}^{U^\chi} = -\frac{\oint \psi_z^{\hat{U}^\chi}(s) t \, \mathrm{d}s}{\oint t \, \mathrm{d}s} \equiv -\frac{\oint \psi_z^{\hat{U}^\chi}(s) \, \mathrm{d}s}{\oint t \, \mathrm{d}s} \quad (\text{if } t \text{ is constant}) \tag{22}$$

As is shown here, the distortional warping function $\psi^{U^\chi}(s)$ can be explicitly determined from the distortion function $\psi^{\chi}(s)$.

4. ONE-DIMENSIONAL FINITE ELEMENT FORMULATION

The one-dimensional potential energy Π may be derived by integrating the potential energy expressed in terms of three-dimensional strain components. As stated earlier, we will consider torsion, torsional warping and only two sets of distortion and corresponding distortional warping ($U^{\chi_1}, U^{\chi_1}, \chi_1$, and χ_2) for the analysis of thin-walled beams having general cross-sections. Omitting the detailed derivation procedure (see [1, 2]), one can show that

$$\Pi = \frac{1}{2} \int \Big\{ E_1 (a_1 U^{\theta'^2} + a_2 U^{\chi_1'^2} + a_3 U^{\chi_2'^2} + 2a_4 U^{\theta'} U^{\chi_1'} + 2a_5 U^{\theta'} U^{\chi_2'}$$

$$+ 2a_6 U^{\chi_1'} U^{\chi_2'}) + E_1 \left(c_1 \chi_1^2 + c_2 \chi_2^2 + 2c_3 \chi_1 \chi_2\right)$$

$$+ G \left(b_1 \theta'^2 + b_2 \chi_1'^2 + b_3 \chi_2'^2 + b_4 U^{\theta^2} + b_5 U^{\chi_1^2} + b_6 U^{\chi_2{}^2}\right)$$

$$+ 2G \left(b_7 U^{\theta} U^{\chi_1} + b_8 U^{\theta} U^{\chi_2} + b_9 U^{\theta} \theta' + b_{10} U^{\theta} \chi_1' + b_{11} U^{\theta} \chi_2'\right.$$

$$\left. + b_{12} U^{\chi_1} U^{\chi_2} + b_{13} U^{\chi_1} \theta' + b_{14} U^{\chi_1} \chi_1' + b_{15} U^{\chi_1} \chi_2' + b_{16} U^{\chi_2} \theta' \right.$$

$$+\ b_{17}U^{\chi_2}\chi_1' + b_{18}U^{\chi_2}\chi_2' + b_{19}\theta'\chi_1' + b_{20}\theta'\chi_2' + b_{21}\chi_1'\chi_2')\ \mathrm{d}z\Big\}$$

$$-\int \left(p_1U^0 + p_2U^{\chi_1} + p_3U^{\chi_2} + q_1\theta + q_2\chi_1 + q_3\chi_2\right)\mathrm{d}z \tag{23}$$

where $(\ )'$ denotes the differentiation with respect to z. Coefficients a_i $(i=1,\ldots,6)$, b_i $(i=1,\ldots,21)$, c_i $(i=1,\ldots,3)$ in Equation (23), which represent the section properties, are given by

$$a_1 = \int_A \left(\psi_z^{U^\theta}\right)^2 \mathrm{d}A, \quad a_2 = \int_A \left(\psi_z^{U^{\chi_1}}\right)^2 \mathrm{d}A, \quad a_3 = \int_A \left(\psi_z^{U^{\chi_2}}\right)^2 \mathrm{d}A$$

$$a_4 = \int_A \psi_z^{U^\theta}\psi_z^{U^{\chi_1}}\,\mathrm{d}A, \quad a_5 = \int_A \psi_z^{U^\theta}\psi_z^{U^{\chi_2}}\,\mathrm{d}A, \quad a_6 = \int_A \psi_z^{U^{\chi_1}}\psi_z^{U^{\chi_2}}\,\mathrm{d}A$$

$$b_1 = \int_A \left(\psi_s^\theta\right)^2 \mathrm{d}A, \quad b_2 = \int_A (\psi_s^{\chi_1})^2\,\mathrm{d}A, \quad b_3 = \int_A (\psi_s^{\chi_2})^2\,\mathrm{d}A$$

$$b_4 = \int_A \left(\frac{\mathrm{d}\psi_z^{U^\theta}}{\mathrm{d}s}\right)^2 \mathrm{d}A, \quad b_5 = \int_A \left(\frac{\mathrm{d}\psi_z^{U^{\chi_1}}}{\mathrm{d}s}\right)^2 \mathrm{d}A, \quad b_6 = \int_A \left(\frac{\mathrm{d}\psi_z^{U^{\chi_2}}}{\mathrm{d}s}\right)^2 \mathrm{d}A$$

$$b_7 = \int_A \left(\frac{\mathrm{d}\psi_z^{U^\theta}}{\mathrm{d}s}\frac{\mathrm{d}\psi_z^{U^{\chi_1}}}{\mathrm{d}s}\right)\mathrm{d}A, \quad b_8 = \int_A \left(\frac{\mathrm{d}\psi_z^{U^\theta}}{\mathrm{d}s}\frac{\mathrm{d}\psi_z^{U^{\chi_2}}}{\mathrm{d}s}\right)\mathrm{d}A, \quad b_9 = \int_A \frac{\mathrm{d}\psi_z^{U^\theta}}{\mathrm{d}s}\psi_s^\theta\,\mathrm{d}A$$

$$b_{10} = \int_A \frac{\mathrm{d}\psi_z^{U^\theta}}{\mathrm{d}s}\psi_s^{\chi_1}\,\mathrm{d}A, \quad b_{11} = \int_A \frac{\mathrm{d}\psi_z^{U^\theta}}{\mathrm{d}s}\psi_s^{\chi_2}\,\mathrm{d}A, \quad b_{12} = \int_A \left(\frac{\mathrm{d}\psi_z^{U^{\chi_1}}}{\mathrm{d}s}\frac{\mathrm{d}\psi_z^{U^{\chi_2}}}{\mathrm{d}s}\right)\mathrm{d}A$$

$$b_{13} = \int_A \left(\frac{\mathrm{d}\psi_z^{U^{\chi_1}}}{\mathrm{d}s}\psi_s^\theta\right)\mathrm{d}A, \quad b_{14} = \int_A \left(\frac{\mathrm{d}\psi_z^{U^{\chi_1}}}{\mathrm{d}s}\psi_s^{\chi_1}\right)\mathrm{d}A, \quad b_{15} = \int_A \left(\frac{\mathrm{d}\psi_z^{U^{\chi_1}}}{\mathrm{d}s}\psi_s^{\chi_2}\right)\mathrm{d}A$$

$$b_{16} = \int_A \left(\frac{\mathrm{d}\psi_z^{U^{\chi_2}}}{\mathrm{d}s}\psi_s^\theta\right)\mathrm{d}A, \quad b_{17} = \int_A \left(\frac{\mathrm{d}\psi_z^{U^{\chi_2}}}{\mathrm{d}s}\psi_s^{\chi_1}\right)\mathrm{d}A, \quad b_{18} = \int_A \left(\frac{\mathrm{d}\psi_z^{U^{\chi_2}}}{\mathrm{d}s}\psi_s^{\chi_2}\right)\mathrm{d}A$$

$$b_{19} = \int_A \psi_s^\theta\psi_s^{\chi_1}\,\mathrm{d}A, \quad b_{20} = \int_A \psi_s^\theta\psi_s^{\chi_2}\,\mathrm{d}A, \quad b_{21} = \int_A \psi_s^{\chi_1}\psi_s^{\chi_2}\,\mathrm{d}A$$

$$c_1 = \int_A n^2\left(\frac{\mathrm{d}^2\psi_n^{\chi_1}}{\mathrm{d}s^2}\right)\mathrm{d}A, \quad c_2 = \int_A n^2\left(\frac{\mathrm{d}^2\psi_n^{\chi_2}}{\mathrm{d}s^2}\right)^2\mathrm{d}A, \quad c_3 = \int_A n^2\left(\frac{\mathrm{d}^2\psi_n^{\chi_1}}{\mathrm{d}s^2}\frac{\mathrm{d}^2\psi_n^{\chi_2}}{\mathrm{d}s^2}\right)\mathrm{d}A$$

Note that these coefficients can be obtained analytically using the shape functions ψ determined in the previous section. One-dimensional load terms p_1, p_2, p_3, q_1, q_2 and q_3 are defined as

$$p_1 = \int_A p\psi_z^{U^\theta}\,\mathrm{d}A, \quad p_2 = \int_A p\psi_z^{U^{\chi_1}}\,\mathrm{d}A, \quad p_3 = \int_A p\psi_z^{U^{\chi_2}}\,\mathrm{d}A$$

$$q_1 = \int_A q\psi_s^\theta\,\mathrm{d}A, \quad q_2 = \int_A q\psi_s^{\chi_1}\,\mathrm{d}A, \quad q_3 = \int_A q\psi_s^{\chi_2}\,\mathrm{d}A$$

where p and q are the external loads in the axial and tangential directions, respectively. Generalized stress resultants H, B, $Q_1, \tilde{B}_1$, Q_2 and $\tilde{B}_2$, which can be described on the boundary, may be defined as

$$H \equiv \int_A \sigma_{zs} \psi_s^{\theta} \, \mathrm{d}A$$

$$B \equiv \int_A \sigma_{zz} \psi_z^{U^{\theta}} \, \mathrm{d}A$$

$$Q_1 \equiv \int_A \sigma_{zs} \psi_s^{U^{\chi_1}} \, \mathrm{d}A$$

$$\tilde{B}_1 \equiv \int_A \sigma_{zz} \psi_z^{U^{\chi_1}} \, \mathrm{d}A$$

$$Q_2 \equiv \int_A \sigma_{zs} \psi_s^{\chi_2} \, \mathrm{d}A$$

$$\tilde{B}_2 \equiv \int_A \sigma_{zz} \psi_z^{U^{\chi_2}} \, \mathrm{d}A$$

Introducing a displacement vector $\mathbf{d}$

$$\mathbf{d}^{\mathrm{T}} = \{\theta, U^{\theta}, \chi_1, U^{\chi_1}, \chi_2, U^{\chi_2}\} \tag{24}$$

One can develop a standard two-node displacement-based C^0-continuous finite element approach based on the energy form (23). The detailed procedure is skipped but a similar procedure can be found in [2].

5. NUMERICAL EXAMPLES

Example 1 (*Cantilever box beam subjected to a couple* (a verification problem)). We consider a cantilever box beam subjected to a couple shown in Figure 5(a) which was treated in earlier investigations [1, 2, 8, 15, 17] ($E = 1.962$ GN/m^2, $v = 0.27$). The magnitude of the two point loads is 4905 N and the magnitude of the resulting torque is 1442.5 N m ($= 4905$ N $\times$ 290 mm). We have followed the three steps described in Section 3 in order to determine the distortion function. The section properties a_i, b_i, and c_i are then computed. Figure 5(b) plots the distortional angles χ for $L/b = 10, 20, 30$. It is clear that the present results agree well with existing results. For rectangular cross-sections one can show that the torsional warping and distortional warping shapes are the same; no distinction between of U^{θ}, U^{χ} is made [2]. Therefore, the one-dimensional displacement vector $\mathbf{d}$ has only three degrees of freedom for torsion, distortion and warping.

Example 2 (*Cantilever beams with general cross sections under a couple*). A cantilever beam with a general cross-section shown in Figure 6(a) is investigated. This is the actual cross-section of an excavator frame pillar ($L = 400$ mm, $t = 2$ mm, $E = 2.0$ GN/m^2, $v = 0.3$, $\rho = 7800$ kg/m^3).

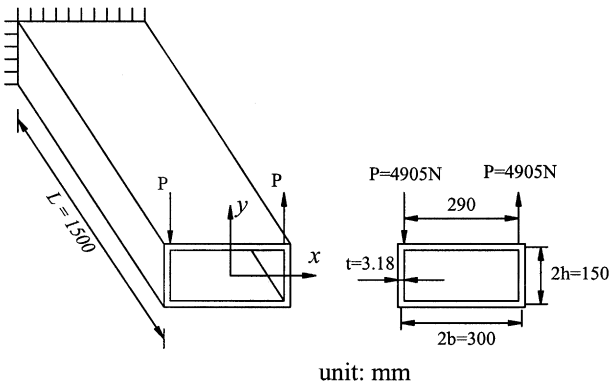

Figure 5(a). A cantilever rectangular box beam subjected to a couple.

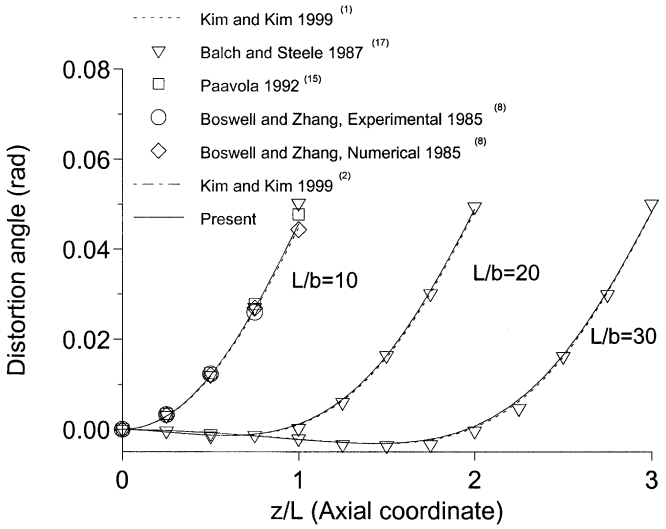

Figure 5(b). Distortion angle along the dimensionless axial co-ordinate.

The same material properties are used in subsequent examples. A couple consisting of two point loads of unit magnitude is imposed on the free edge of the beam.

For this problem, two sets of distortion and distortional warping deformation functions should be used; therefore the one-dimensional displacement vector has six degrees of freedom (see Equation (24)). Figure 6(b) shows the axial distribution of u_y (displacement in y) along the edge ($x = 50$ mm, $y = 0$ mm). We compare the results by the use of only one set of distortion and distortional warping deformation shapes with those by the use of two sets of distortion and distortional warping shapes. The NASTRAN [18] *plate* element results are regarded as the

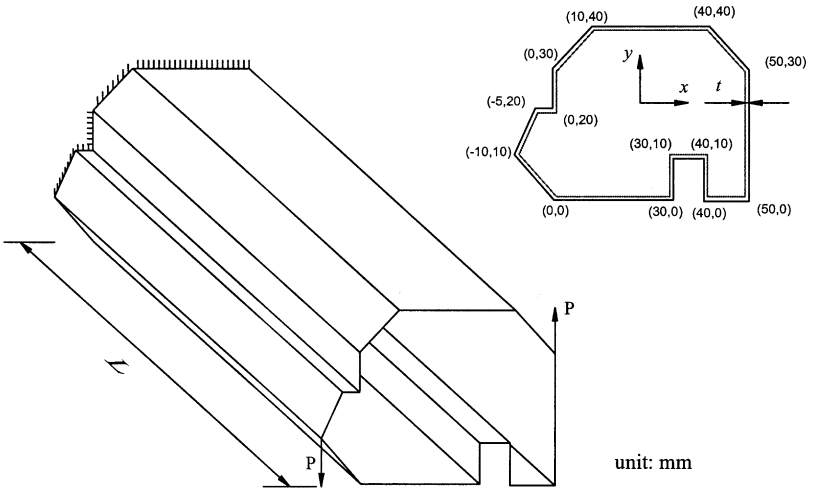

Figure 6(a). A cantilever beam representing an excavator pillar, which is subjected to a couple.

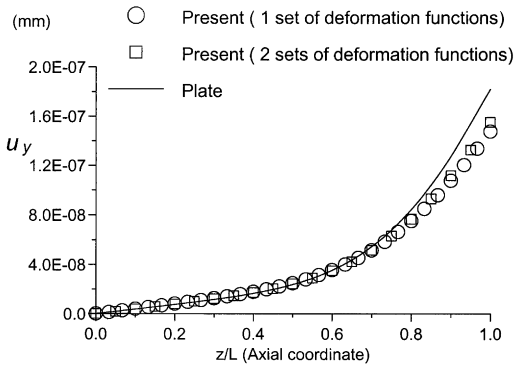

Figure 6(b). The axial variation of the displacement u_y in the y direction at $x = 50$ mm, $y = 0$ mm.

reference results for this problem. It is clear that the analysis with only one set of distortion and distortional warping deformation functions gives quite satisfactory results.

The importance of using two sets of deformation functions is apparent in the following example. Here, we consider a typical cross-section of an automobile pillar shown in Figure 7(a). This cross-section was used by Nikolaidis and Zhu [19], who studied the characteristics of automotive joints. The boundary and loading conditions are the same as those of the previous example ($L = 1500$ mm, $t = 2$ mm). The displacement u_y is plotted along $x = 86.1$ mm, $y = -138.8$ mm in Figure 7(b) as the function of the axial co-ordinate. In this case, the results using only one set of distortion and distortional warping deformation functions produce significant errors while the analysis using two sets gives results favourable with those from the plate finite element analysis. This example

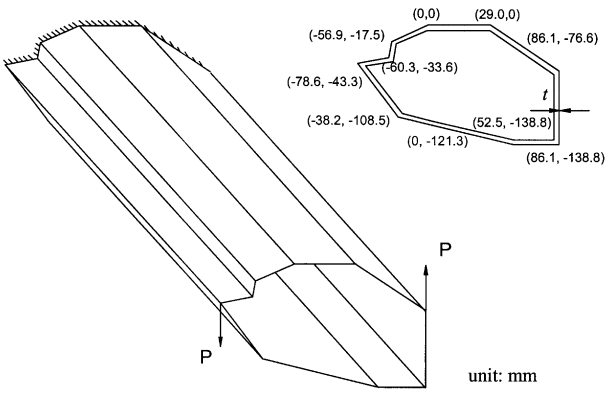

Figure 7(a). A cantilever beam representing a typical automobile pillar, which is subjected to a couple.

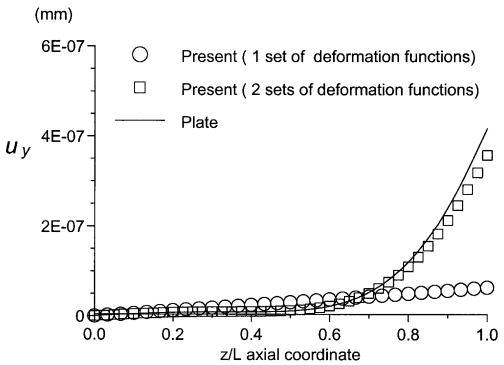

Figure 7(b). The axial variation of the displacement u_y in the y direction at $x = 86.1$ mm, $y = -138.8$ mm.

illustrates that at least two pairs of distortion and distortional warping shapes are required in the coupled torsion-distortion-warping analysis of thin-walled closed beams having general cross-sections. The analysis on other cross-sections also confirmed the present argument, although not included in the present work.

Example 3 (*Free vibration analysis for general cross sections*). In this example, we carry out the vibration analysis of freely supported beams shown in Figures 6(a) and 7(a). The first distortional and torsional eigenfrequencies obtained from the present one-dimensional analysis are compared in Tables I and II with those obtained from the plate finite element analysis. The corresponding eigenmodes are plotted in Figures 8 and 9, which agree with those by the NASTRAN plate element analysis (NASTRAN results are not plotted).

Note that the mode shapes plotted in Figures 8 and 9 are reconstructed from the one-dimensional analysis. It is also remarked that the mode shapes in these problems are neither purely distortion

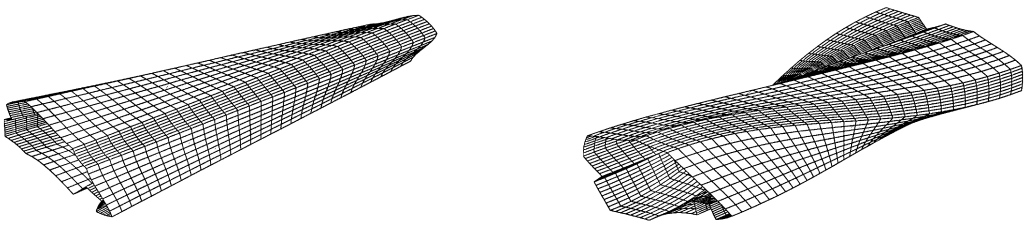

(a) (b)

Figure 8. (a) The first distortional; and (b) torsional eigenmodes of a freely supported beam shown in Figure 6(a).

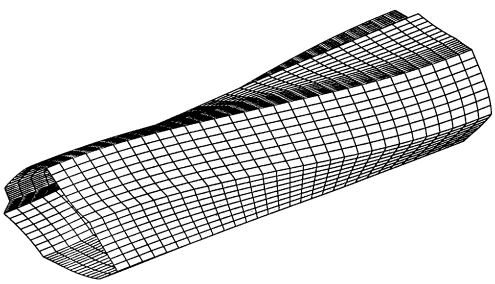

Figure 9. The first torsional eigenmode of a freely supported beam shown in Figure 7(a).

Table I. Eigenfrequencies of a freely supported beam shown in Figure 6(a)*.

Mode shape	Plate ($N_\varepsilon = 2278$)	Present ($N_\varepsilon = 10$)	Present ($N_\varepsilon = 30$)
Distortion dominant (Figure 8(a))	1374.5 HZ	1348.3 HZ	1348.1 Hz
Torsion dominant (Figure 8(b))	3131.5 Hz	3148.3 Hz	3135.0 Hz

*(N_ε: the number of the present elements.)

Table II. Eigenfrequencies of a freely supported beam shown in Figure 7(a).

Mode shape	Plate ($N_\varepsilon = 2728$)	Present ($N_\varepsilon = 10$)	Present ($N_\varepsilon = 30$)
Torsion dominant (Figure 9)	958.1 Hz	969.4 Hz	965.8 Hz

nor purely torsional. As evident in Tables I and II, the present one-dimensional analysis gives very satisfactory results even in complex beam cross-sections.

6. CONCLUSIONS

We proposed a new theory for a one-dimensional analysis of thin-walled closed beams having general cross-sections. A semi-analytic beam-frame approach was proposed to determine the

sectional deformations of the cross-section. It is also argued that the minimum number of distortional deformation functions is two for general cross-sections having more than four edges. The practical usefulness of the present one-dimensional analysis was demonstrated for beams having general cross-sections including automobile and excavator pillar sections.

REFERENCES

1. Kim YY, Kim JH. Thin-walled closed box beam element for static and dynamics analysis. *International Journal for Numerical Methods in Engineering* 1999; **45**:473–490.
2. Kim JH, Kim YY. Analysis of thin-walled closed beams with general quadrilateral cross sections. *ASME Journal of Applied Mechanics* 1999; **66**(4):904–912.
3. Vlasov VZ. *Thin Walled Elastic Beams*. Israel Program for Scientific Translations, Jerusalem, 1961.
4. Maisel BI, Roll F. Methods of analysis and design of concrete boxbeams with side cantilevers. *Technical Report*, Cement and Concrete Association, London, 1974.
5. Maisel BI. Analysis of concrete box beams using small-computer capacity. *Development Report* 5, Cement and Concrete Association, London, 1982.
6. Bažant ZP, Nimeiri ME. Stiffness method for curved box girders at initial stress. *Journal of the Structural Division* 1974; **100**(ST10):2071–2090.
7. Boswell LF, Zhang SH. A box beam finite element for the elastic analysis of thin-walled structures. *Thin-Walled Structures* 1983; **1**:353–383.
8. Boswell LF, Zhang SH. An experimental investigation of the behavior of thin-walled box beams. *Thin-Walled Structures* 1985; **3**:35–65.
9. Zhang SH, Lyons LPR. A thin-walled box beam finite element for curved bridge analysis. *Computers and Structures* 1984; **18**(6):1035–1046.
10. Zhang SH, Lyons LPR. The application of the thin-walled box beam element to multibox bridge analysis. *Computers and Structures* 1984; **18**(5):795–802.
11. Razaqpur AG, Li HG. Thin-walled multicell box girder finite element. *Journal of Structural Engineering ASCE* 1991; **117**(10):2953–2971.
12. Razaqpur AG, Li HG. A finite element with exact shape functions for shear lag analysis in multi-cell box-girders. *Computers and Structures* 1991; **39**(1/2):155–163.
13. Razaqpur AG, Li HG. Refined analysis of curved thin-walled multicell box girders. *Computers and Structures* 1994; **53**(1):131–142.
14. Mikkola MJ, Paavola J. Finite element analysis of box girders. *Journal of the Structural Division ASCE* 1980; **106**(ST6):1343–1357.
15. Paavola J. A finite element technique for thin-walled girders. *Computers and Structures* 1992; **44**(1/2):159–175.
16. Boswell LF, Zhang SH. The effect of distortion in thin-walled box-spine beams. *International Journal of Solids and Structures* 1984; **20**(9/10):845–862.
17. Balch CD, Steele CR. Asymptotic solutions for warping and distortion of thin-walled box beams. *ASME Journal of Applied Mechanics* 1987; **54**:165–173.
18. MSC/NASTRAN. *User's Manual*. The McNeal Schwendler Corporation, Los Angeles, 1989.
19. Nikolaidis E, Zhu M. Design of automotive joints: using neural networks and optimization to translate performance requirements to physical design parameters. *Computers and Structures* 1996; **60**(6):989–1001.

